# Multi-mode Failure Analysis of Scratched Laminated Carbon Fiber/Epoxy Composites

*Seyedmohammad S. Shams, Rani F. El-Hajjar[*]*
*[*]Corresponding Author, Department of Civil Engineering and Mechanics,*
*3200 North Cramer St., College of Engineering & Applied Science*
*University of Wisconsin, Milwaukee, WI 53217, USA*
*Contact: E-mail: elhajjar@uwm.edu (R. F. El-Hajjar)*
*Tel: 1-414-229-3647, Fax: 1-414-229-6958*

*Abstract: Composite structures can be vulnerable to several types of damage. Abrasion and low to mid velocity impacts can result in deep scratches impacting the surface plies. In this study, the delamination which is induced by scratches under tensile loading are investigated using experimental and finite element techniques. A finite element approach based on progressive damage analysis implemented in VUMAT subroutine and a cohesive zone model using Abaqus are performed to simulate the behavior in the composite specimen. Scratches at different depths with different angles in carbon fiber-epoxy laminates are modeled to study the influence of the scratch size and the stacking sequence effects. Experimental results show the delamination propagates between layers. The results prove that the scratch tip location and size control the load carrying capacity as a result of the delamination response originating in undesirable bending and torsional deformations.*

*Keywords: Laminated Composites; Fracture mechanics; Hashin failure criterion; Cohesive Behavior; Failure Theory*

# 1. Introduction

Laminated fiber-reinforced composites have been increasingly used due to their relatively high specific strength and stiffness but more importantly for their flexibility in design and performance. Different mechanical properties might be achievable by plies stacking in different directions considering symmetric and asymmetric features. Serious failures in composite structures can occur due to the presence of manufacturing flaws not detected in manufacturing or due to mechanical impact damage in the course of service [1, 2]. Manufacturing flaws can result in significant reductions in strength and stiffness of composites [2-5]. Delamination can occur at processing defects or in-service at stress concentrators such as holes, ply-drop-offs, stringer run-outs, etc.[6]. In aerospace structures, in-service damage can be classified into low to high velocity impacts. Low velocity impact caused by ice/concrete pieces and stones that impact the structure during takeoffs and landings, bird strikes. During course of ground maintenance operations, the probability of low velocity impacts and abrasion by dropping tools and ladders are very high. Figure 1 shows an example of a deep scratch on a composite panel.


**Figure 1 Scratch type damage in a composite structure [7]**

Metals have proper capability to absorb impacts by plastic deformation mechanism, but in contrast with metals, the high-strength composites, such as boron and carbon fiber reinforced plastics, result in different damage morphologies involving fiber and matrix failures. Therefore, composite structures cannot prevent this type of scratch induced damage from occurring [7]. Aerospace structure usually employs very thin cross-sections in large areas of the body. Consequently, these damages can affect the structural load-bearing capability of the composite structure.

Composite structures design needs to be evaluated by damage analysis of any possible defects. Therefore, scratch damage analysis and its effects on failure probability of composite structures are primary for designing safe and optimized. Continuum damage mechanics and fracture mechanics approaches have been proposed to determine the onset and propagation of delamination which are critical for structural integrity assessment of composite structures. Besides those earlier approaches, the virtual crack closure technique (VCCT) and cohesive zone model (CZM) have been successfully used to predict the failure in composite structures. The simulation of progressive delamination using cohesive elements has been modeled using the concepts of damage, softening and fracture mechanics. This approach need not have an initial crack thereby allowing the possibility to predict the onset and propagation of a crack in the cohesive zone. In a finite element model using the cohesive zone model, guidelines have been proposed for selecting element size, stiffness and strength of the cohesive zone.  Turon et al. [8] proposed a procedure which accounts for the size of a cohesive finite element and the length of the cohesive zone to ensure the correct dissipation of energy. Diehl [9] developed a novel penalty methodology for enhancing the use of the cohesive zone model in finite element models.

This study presents a complete failure analysis of scratched carbon-fiber/epoxy composites. The overall objective is to investigate the effects of scratches on strength of composite laminates. These scratches or "gouges" investigated impact different depths of the composite laminates.  A CZM finite element model coupled with a progressive damage model is used to model the failure behavior of the tested specimens.  The proposed approach is used to investigate the effects of the scratch depth and its size effects on delamination failure response.

## 2. Modeling approach

The finite element and experiment are constructed based on a schematic archetype of a tensile test. Figure 2 illustrates a scratched composite laminate model which is damaged by a virtual scratch. The scratch effects are studied in tension coupons and by using wedge shaped features in the middle of specimens.

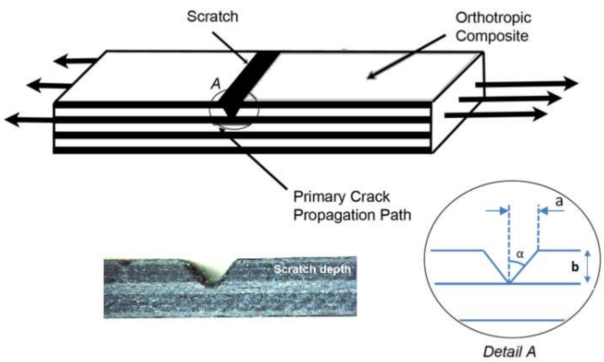


**Figure 2 Geometry of scratched tension specimen in gage section**

A Cohesive Zone Model and 3D composite material micro-failure theory within Abaqus [10] finite element software are used to model the crack initiation and propagation . The basic concepts of Cohesive Zone Model (CZM) were presented by Barenblatt [11]. The CZM principle was implemented in the finite element framework by Hillerborg et al [12]. The interface in CZM is modeled as a constitutive behavior specified by a traction-separation relationship. The CZM approach assumes that a cohesive damage zone, or softening evolution, develops near the crack tip. The derivation and finite element implementation of the cohesive damage model are described in [13]. In a CZM model, a constitutive law for the interface relates traction, $T$, to the distance jump between two surfaces of the crack, $\delta$, by structural operator, C, on a plane of separation:

$$\mathrm{T} = \mathrm{C}\delta \qquad (1)$$

The energy dissipated in the process of fracture at final fracture displacement computed by:

$$\int_0^{\delta_f} \mathrm{T}\,\mathrm{d}\delta = \mathrm{G_C} \qquad (2)$$

Where, $\mathrm{G_C}$ is the area under the curve defined by equation that represents the energy required for complete failure of the interface. Figure 3 shows this concept for pure mode I, which can be developed for other shear and transverse modes.

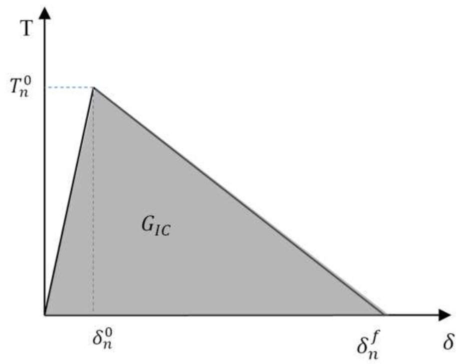


**Figure 3 Bilinear traction-separation under mode I**

Traction-separation laws are described by using a damage initiation criterion and a damage evolution law. There are various criterions using an interaction between the components of tractions or displacements in different modes to predict crack initiation. For the crack evolution which is known as propagation, these criterions are governed by energy release rate components. The interfacial tractions for different modes are:

$$T_n = \frac{\partial \emptyset}{\partial \delta_n}, T_t = \frac{\partial \emptyset}{\partial \delta_t}, T_s = \frac{\partial \emptyset}{\partial \delta_s} \quad (3)$$

Where $\emptyset$ is the potential function of the cohesive zone. The value of interfacial separation at the point of damage initiation is, $\delta^0$. At a value of displacement,$\delta^f$, damage is completed and beyond this point the interfacial traction remains zero. The evolution laws for the damage threshold and the damage variable must be defined in the damage model. A bilinear T−δ relationship by definition of the damage variable, D, is defined:

$$D = \frac{\delta^f(\delta-\delta^0)}{\delta(\delta^f-\delta^0)} \quad (4)$$

"D" evolves from 0 to 1 upon further loading after initiation of damage. This is a model which is currently implemented in the Abaqus [10] and is based on formulations proposed by Camanho [14]. The following propagation criterion are used within the relationship for the total critical strain energy release rate, $G_{TC}$, and components of mixed-mode evolution [15], [16]:

$$G_{TC} = G_{Ic} + (G_{IIc} - G_{Ic})\left(\frac{G_{shear}}{G_T}\right)^{\gamma} \quad (5)$$

Where $G_{Ic}$ is critical mode-I strain energy release rate, $G_{IIc}$ is the critical mode-II strain energy release rate. $G_{shear}$ is the shear energy release rate in a mixed mode loading case and $\gamma$ is a cohesive property. In the modeling approach, a cohesive interface technique is used to simulate the delamination between layers on the scratch region after confirmation with experimentally observed behavior of the delamination path in the scratch region. The progressive damage analysis model used relies on a combination of Hashin's failure criteria [17] and Puck's action plane theory [18]. The validity of these theories against experimental results have been previously documented [19].

These two methodologies are implemented within an explicit finite element analysis for modeling the scratch damage effects. A 3D linear brick element is used which allows for specification of the transverse shear effects in the out of plane direction of each ply. The damage progression model of this approach containing the Hashin's criteria and Puck's action plane models are implemented as a user subroutine ,VUMAT [20]. In these models, the following are the definitions of the damage variables:

Tensile fiber failure: $\sigma_{11} > 0$

$$e_f^t = \left(\frac{\sigma_{11}}{F_1^{tu}}\right)^2 + \left(\frac{\sigma_{12}}{F_{12}^{su}}\right)^2 + \left(\frac{\sigma_{13}}{F_{13}^{su}}\right)^2 = 1 \quad (7)$$

Compressive fiber failure: $\sigma_{11} < 0$

$$e_f^c = \frac{|\sigma_{11}|}{F_1^{cu}} = 1 \quad (8)$$

The tensile and compressive matrix failures modes are:

$$\left[\left(\frac{\sigma_{11}}{2F_1^{tu}}\right)^2 + \frac{\sigma_{22}{}^2}{|F_2^{tu}.F_2^{cu}|} + \left(\frac{\sigma_{12}}{F_{12}^{su}}\right)^2\right] + \sigma_{22}\left(\frac{1}{F_2^{tu}} + \frac{1}{F_2^{cu}}\right) = 1 \qquad (9)$$

$$\sigma_{22} + \sigma_{33} > 0;\ \text{then } e_m^t = 1 \qquad (10)$$

$$\sigma_{22} + \sigma_{33} < 0;\ \text{then } e_m^c = 1 \qquad (11)$$

In the above relations, the damage variables $e_f^t$ , $e_f^c$, $e_m^t$, $e_m^c$, are associated with the fiber and matrix in tension and compression failure modes respectively. When damage variables are met to one for each element, the element is removed. $F_1^{tu}$, $F_1^{cu}$, and $F_2^{tu}$, $F_2^{cu}$, are the tensile and compressive failure stresses in fiber and transverse directions respectively and $F_{12}^{su}$, $F_{13}^{su}$ are corresponded to failure shear stresses in shear and transverse plane respectively. Transient dynamic models using an explicit FE solver were used to model the scratch specimens to improve solution robustness and convergence during the failure progression [10]. A ply-by-ply 3D analysis technique is utilized to model the laminated carbon/fiber composite. Three-dimensional solid elements are used to capture the interlaminar stresses around the scratch zone. The models consist of 52,988 three-dimensional 8-node Abaqus C3D8I solid for cohesive zone model. As the VUMAT subroutine which is used to perform Hashin criterion for solid element is compatible with C3D8R element type, these elements are used for combination of Hashin's criterion and cohesive contact model.

Cohesive zone model as a cohesive contact and Hashin model as implemented in a VUMAT subroutine are combined in a final model. The simulation is performed under high performance parallel computing in a cluster service. In order to use Abaqus 6.10-EF1on the cluster a script is provided to simplify the interface. The models have been used two cluster nodes (16 processors and 48 gibibytes of RAM) utilizing MPI (Message Passing Interface) for 10 hours.

The properties of the unidirectional carbon/epoxy composite and the properties of the interface are shown in Tables 1, respectively. Note that in this table, $F_1$ and $F_2$ refer to the axial and transverse properties respectively and the superscripts, T and C refer to tension and compression properties.

**Table 1 Orthotropic mechanical properties and interfacial properties of the carbon/epoxy T700GC-12K-31E / #2510 Prepreg[21]**

| $E_1$ **GPa (Msi)** | $E_2$ **GPa (Msi)** | $\nu_{12}$ | $G_{12}$ **GPa (Msi)** | $F_1^{tu}$ **GPa (ksi)** | $F_2^{tu}$ **GPa (ksi)** | $F_1^{cu}$ **GPa (ksi)** | $F_2^{cu}$ **GPa (ksi)** | $F_{12}^{su}$ **GPa (ksi)** | $G_{Ic}$ **Jm$^{-2}$ (lb/in)** | $G_{IIc}$, $G_{IIIc}$ **Jm$^{-2}$ (lb/in)** | $T_n$, $T_t$, $T_s$ **GPa (ksi)** |
|---|---|---|---|---|---|---|---|---|---|---|---|
| 125 (18.1) | 8.40 (1.23) | 0.309 | 4.22 (0.613) | 2.16 (314.4) | 0.049 (7.09) | 1.45 (209.1) | 0.20 (28.8) | 0.15 (22.4) | 217 (1.26) | 586 (3.35) | 0.049 (7.09) |

The values of Mode II and mode III were assumed to be equal [22]. Nominal thickness of each ply is approximately 0.15 mm (0.006 in). Finite element models for various layup and depth of scratches are built. In this study, the models contained 3 ply, 4 ply and 5 ply deep scratches. The analysis has shown that the wedge angle of the scratch influences the onset and propagation of the crack near the tip of the scratch. Therefore, the models with different depth of scratches are designed to have a constant wedge angle at the scratch zone. For the scratch size or depth investigations, this angle is changed corresponding to the geometry of the scratch (Figure 2). The location of scratches is designed to be at the interface ply. This feature supports the experiment and analysis to be more accurate to take the stacking sequence and size effect into account. Experimental evidences rely on detecting the initiation and propagation at the ply interface.

## 3. Experimental methods

Pre-impregnated carbon fiber/epoxy unidirectional composite layers for making the test specimens are used. After tailoring and stacking up in appropriate directions, the specimens were cured using a hot-press. This approach utilizes uniform heat and pressure according to the recommended 121 degrees Celsius (250 degrees Fahrenheit) cure cycle. The fiber and epoxy used to make these specimens were fabricated from a Toray prepreg T700GC-12K-31E fiber with the #2510 epoxy system [21]. Table 1 shows the material properties. The laminated plates manufactured were 280 mm x 280 mm (11.0 x 11.0 inch). The layup investigated was a $[0/45/90/-45/0]_s$ and was selected due to its common standard use as well as its ability to generate different interfaces near the scratch zone that was varied for different tests[7].

The final specimens are cut from prepared panels. A single end 90-degree solid micro grain carbide chamfer mill tool was used to make the scratches on the cured panel by using a Computer Numerical Control (CNC) knee milling machine. The tool has a cutter size of 0.79 mm (0.0312 in) and is coated by Titanium to ensure the lowest probability of pre-deboning plies during the manufacturing process. The CNC machine is programmed to find the panel center and travel across the length of panel perpendicular to the fiber directions on the top face. The milling process is automated feed for 10 steps in particular depth of 0.076 mm (0.003 in) in each step. The specimens were tested in tension according to the ASTM D3039 [23] standard for tensile properties of polymer reinforced fiber composites. The experiments were performed in a displacement control mode. The load was applied using an electromechanical test system with a 200 kN (22 kips) capacity and extensometer for recording the deformation behavior. The maximum error of the recorded load was within ±0.02 kN (5 lb).

## 4. Results and Discussion

The experimental and FE results show the crack growth onset occurs at low load levels followed by unstable crack propagation. The unstable progressive delamination exposed by experiments discloses a significantly different failure mode from specimens with no scratches. An observations of a pristine multidirectional specimen tested in tension reveal that the failure occurs across the specimen and results in multiple failures which involve the entire specimen from the center of the specimen to the grip region. Note the test data presented is restricted to the results occurring until the delamination reaches the grip region after which the test is terminated. Figure

4 shows how the delamination initiates on the corner of the specimen and suddenly propagates across the entire specimens.

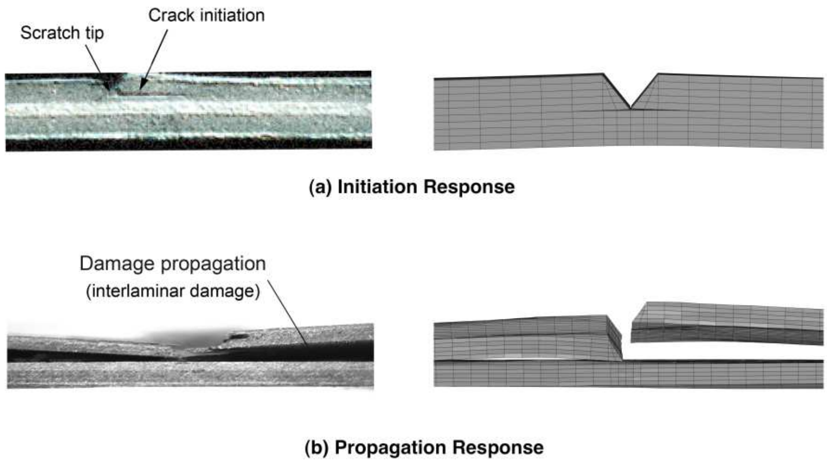


**Figure 4 Micrograph showing scratch initiation and propagation of damage[7]**

The initiation stage is driven as singularities dominate the local response of the laminate near the scratch tip. The size or depth of the scratches plays an important role at this stage. A survey of the classical composite laminate theory displays that the local loss of symmetry in the laminate in the scratch region induces an obvious bending and twisting deformations. Abaqus simulations correlate with evidences from experiments. As the delamination propagates in the specimen, Figure 5 shows the delamination is not symmetric across the width of specimen as well as toward the applied load and clamped side. The test observations from all specimens with 3 ply, 4 ply and 5 ply deep scratches show a similar response.

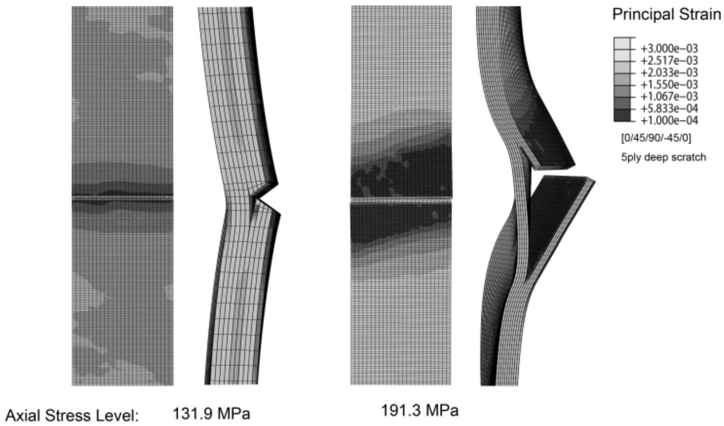


**Figure 5 Plot of finite element model showing (a) bending and (b) twisting moments at crack initiation and propagation for a specimen with a 5-ply deep scratch[7]**

The proposed models for scratch behavior show that the delamination initiation and propagation are stimulated by a mixed-mode mechanism. Since, the proposed FE modeling framework utilizes 3D elements considering out of plane stresses, it can capture mixed-mode tractions and fracture energies. Figure 6 shows the prediction of delamination by using the Hashin criterion and cohesive zone while also considering the cohesive model alone. In this model the percentage of linear error for the average results of experimental analysis relative to Hashin model is 2%. Figure 7 illustrates the capability of CZM modeling using cohesive contact to predict damage initiation and propagation. Even the error is more than combined modeling, it still predicts well. In this study, the scratch size is modeled based on the geometry that is shown in Figure 2. By increasing wedge angle, a/b increases. Consequently, the stress concentration at the scratch tip increases which reduces the maximum failure load. Figure 8 shows how the scratch size affects the load-displacement curve.

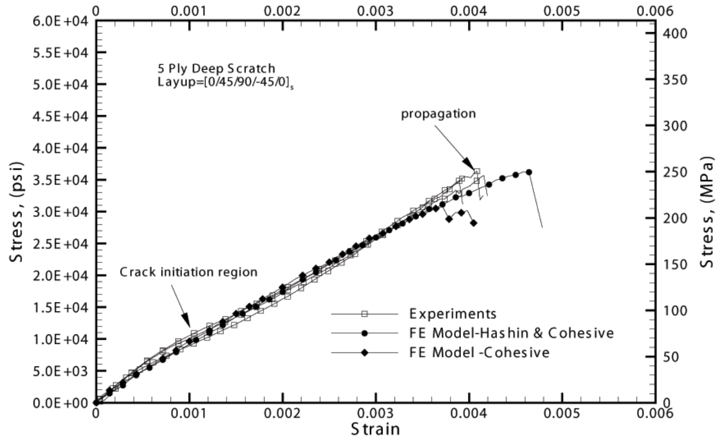


**Figure 6 Model predictions for 10ply laminates with 5 ply deep scratch**

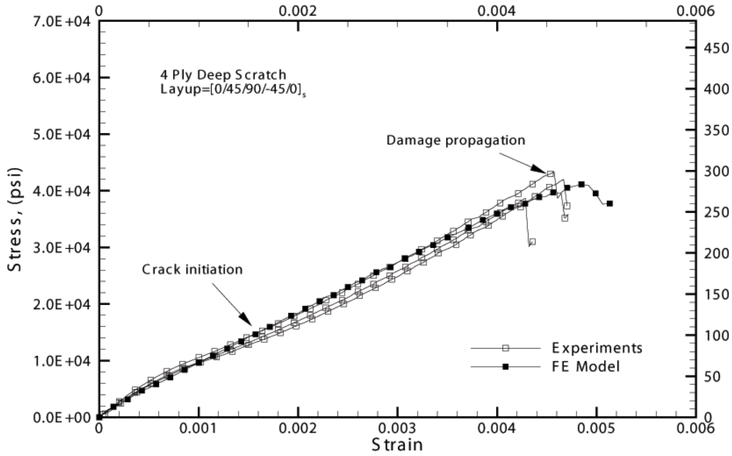


**Figure 7 Model predictions for 10ply laminates with 4 ply deep scratch**

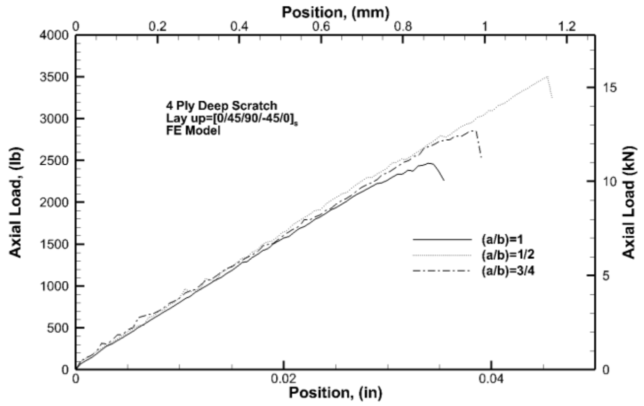


**Figure 8 Scratch size effect investigations for 4 ply deep scratch**

**Table 3 Predicted damage propagation loads compared to experimental results**

| Depth of Scratch | $P_{Dp}$ (Average of Experiments) KN (lb) | $P_{Dp}$ (Predicted FE Models) KN (lb) | Error % |
|---|---|---|---|
| **3 ply** | 11.819 (2657.2) | 12.501 (2810.5) | 5.7 |
| **4 ply** | 10.975 (2467.3) | 10.923 (2455.8) | 0.5 |
| **5 ply** | 9.386 (2110.1) | 8.226 (1890.2) | 10.5 |

Damage propagation load, $P_{Dp}$, is predicted by using CZM models for various scratch depth shown in Figure 3. The examined stacking sequence is $[0/45/90/-45/0]_s$. Predictions are influenced by the scratch size. A 5ply deep scratch has a larger size of scratch where even the wedge angle is the same for all specimens with different depths. The loads are also influenced by the, asymmetric level of impacted laminate and stacking sequence at the scratch depth. Table 4 shows the effect of ply stacking sequence that is investigated for different layup in 4 ply deep scratch specimens. $P_{D_i}$ is the tensile load in which the damage has been initiated. It should be noted that the laminate stiffness for various stacking sequence are different. From these results it is observed that the material failure wasn't the dominant failure mode before interlaminar delamination with the behavior primarily captured by the cohesive models. The simulations show the initiation and propagation of delamination to be captured by the cohesive zone model and the damage mechanics approaches have proper correlation with experiments.

**Table 4 Initiation and propagation failure loads for different stacking sequences (4 ply deep scratch)**

| Stacking sequence | Interface | $P_{Di}$ KN (lb) | $P_{Dp}$ KN (lb) | $P_{Di}$ /$P_{Dp}$ |
|---|---|---|---|---|
| $[45/-45/90/0/0]_s$ | 0/0 | 5.673 (1275.4) | 11.746 (2640.7) | 0.48 |
| $[0/45/90/-45/0]_s$ | -45/0 | 4.437 (957.3) | 10.923 (2455.8) | 0.38 |
| $[0/45/-45/90/0]_s$ | 90/0 | 3.144 (706.9) | 10.698 (2405.2) | 0.29 |

## 5. Conclusions

Scratch defects can significantly change the composite laminate behavior under tension. These changes can be induced by two important stages during the failure process. The first debond at the edge of the scratch profile occurs due to free edge effects and high stress concentration where the scratch tip intersects with free edge of laminate. Scratch size effects are involved with this stage of failure. Relatively large bending and twisting moments occur in the induced asymmetric conditions which the scratched laminate experiences after crack initiation. These large deformation modes result in high interlaminar stresses causing unstable progressive delaminations to form near the scratch tip. While the damage approach did not show significant response in these models, it may become more important in thicker laminates. The proposed FE modeling approach is shown to be able to model the behavior of laminates with different levels of scratch depths, size and stacking sequences. It is also able to account for both the delamination and continuum assumed material failure modes,

## 6. References


1. Riskalla, P.M.G.a.M.G., Development of Probabilistic Design Methodology for Composite Structures, August 1997, Vought Aircraft Company,DOT/FAA/AR-95/17.
2. El-Hajjar, R.F. and D.R. Petersen, Gaussian function characterization of unnotched tension behavior in a carbon/epoxy composite containing localized fiber waviness. Composite Structures, 2011. 93(9): p. 2400-2408.
3. Huang, H. and R. Talreja, Effects of void geometry on elastic properties of unidirectional fiber reinforced composites. Composites Science and Technology, 2005. 65(13): p. 1964-1981.
4. Hsiao, H.M. and I.M. Daniel, Elastic properties of composites with fiber waviness. Composites Part a-Applied Science and Manufacturing, 1996. 27(10): p. 931-941.

5. Soutis, C. and J. Lee, Scaling effects in notched carbon fibre/epoxy composites loaded in compression. Journal of Materials Science, 2008. 43(20): p. 6593-6598.
6. Ratwani, M.M., Effect of Damage on Strength and Durability. NATO Research and Technology Organisation, May 2010 RTO-EN-TR-AVT-156 AC/323(AVT-156)TP/333
7. Shams, S.S. and R.F. El-Hajjar, Effects of Scratch Damage on Progressive Failure of Laminated Carbon Fiber/Epoxy Composites. International Journal of Mechanical Sciences, 2013. In press.
8. Turon, A., C.G. Dávila, P.P. Camanho, and J. Costa, An engineering solution for mesh size effects in the simulation of delamination using cohesive zone models. Engineering Fracture Mechanics, 2007. 74(10): p. 1665-1682.
9. Ted, D., On using a penalty-based cohesive-zone finite element approach, Part I: Elastic solution benchmarks. International Journal of Adhesion and Adhesives, 2008. 28(4-5): p. 237-255.
10. Abaqus, Abaqus 6-11EF, in Dassault Systems2011, Simulia.
11. G.I, B., The Mathematical Theory of Equilibrium Cracks in Brittle Fracture, in Advances in Applied Mechanics, T.v.K.G.K.F.H.v.d.D. H.L. Dryden and L. Howarth, Editors. 1962, Elsevier. p. 55-129.
12. A. Hillerborg, M.M., P.E. Petersson, Analysis of crack formation and crack growth in concrete by means of fracture mechanics and finite elements. Cement and Concrete Research, 1976. 6, 773-782.
13. Turon, A., P.P. Camanho, J. Costa, and C.G. Dávila, A damage model for the simulation of delamination in advanced composites under variable-mode loading. Mechanics of Materials, 2006. 38(11): p. 1072-1089.
14. Pedro P Camanho, C.G.D., Mixed-Mode Decohesion Finite Elements for the Simulation of Delamination in Composite Materials. NASATechnical Paper, 2002.
15. Camanho P.P., D.a.C.G., de Moura M.F. , Numerical Simulation of Mixed-Mode Progressive Delamination in Composite Materials. Journal of Composite Materials, 2003. 37 (16), 1415-1438.
16. Benzeggagh, M.L. and M. Kenane, Measurement of mixed-mode delamination fracture toughness of unidirectional glass/epoxy composites with mixed-mode bending apparatus. Composites Science and Technology, 1996. 56(4): p. 439-449.
17. Hashin, Z., Failure Criteria for Unidirectional Fiber Composites. Journal of Applied Mechanics, June 1980. Volume 47, Issue 2, 329 (6 pages).
18. Puck, A. and H. Schürmann, FAILURE ANALYSIS OF FRP LAMINATES BY MEANS OF PHYSICALLY BASED PHENOMENOLOGICAL MODELS. Composites Science and Technology, 1998. 58(7): p. 1045-1067.
19. Hinton, M.J., A.S. Kaddour, and P.D. Soden, A comparison of the predictive capabilities of current failure theories for composite laminates, judged against experimental evidence. Composites Science and Technology. 62(12-13): p. 1725-1797.
20. Simulia, Abaqus/Explicit VUMAT for the simulation of damage and failure in unidirectional fiber composite materials. Abaqus VUMAT, July 2011.

21. Tomblin J, S.J., Seneviratne W, Raju KS, , Advanced General Aviation Transport Experiments. A – Basis and B – Basis Design Allowables for Epoxy – Based Prepreg TORAY T700GC-12K-31E/#2510 Unidirectional Tape, 2002, National Institute for Aviation Research Wichita State University: Wichita, Kansas.
22. Daniel, I. and O. Ishai, Engineering Mechanics of Composite Materials. Vol. Second edition. 2006: Oxford University Press.
23. ASTM, Standard test method for tensile properties of polymer matrix composite materials, 2007, ASTM International: West Conshohocken, PA.